AMERICAN SOCIETY FOR MICROBIOLOGY | Molecular and Cellular Biology

Role of Src Family Kinases in Regulation of Intestinal Epithelial Homeostasis

Shinya Imada,[a,b] Yoji Murata,[a] Takenori Kotani,[a] Masaki Hatano,[a] Chunxiao Sun,[a] Tasuku Konno,[a] Jung-ha Park,[a]* Yasuaki Kitamura,[a] Yasuyuki Saito,[a] Hideki Ohdan,[b] Takashi Matozaki[a]

Division of Molecular and Cellular Signaling, Department of Biochemistry and Molecular Biology, Kobe University Graduate School of Medicine, Kobe, Japan[a]; Department of Gastroenterological and Transplant Surgery, Applied Life Sciences, Institute of Biomedical & Health Sciences, Hiroshima University, Hiroshima, Japan[b]

Proper regulation of epithelial cell turnover is important for the structural integrity and homeostasis of various tissues, including the intestine. Here we show that ablation of Csk, a negative regulator of Src family kinases (SFKs), specifically in intestinal epithelial cells (IECs) resulted in the development of hyperplasia throughout the intestinal epithelium of mice. Such conditional ablation of Csk also increased the proliferative activity and turnover of IECs, disturbed the differentiation of Paneth and goblet cells, reduced the number of intestinal stem cells, and attenuated the expression of Wnt target genes in the intestine. Moreover, the tyrosine phosphorylation of focal adhesion kinase (FAK) and the activities of both Rac and Yes-associated protein (YAP) were increased in intestinal crypts or organoids of the mutant mice, whereas inhibition of Rac or YAP activity rescued the mutant phenotypes. Our results thus suggest that SFKs promote the proliferation of IECs in intestinal crypts through activation of Rac or YAP and that they thereby contribute to the proper regulation of IEC turnover and intestinal homeostasis.

Terminally differentiated and mature cells possess a distinct life span that is strictly regulated in order to achieve and maintain homeostasis and structural integrity in a variety of tissues and organs. The life span of intestinal epithelial cells (IECs)—in particular, that of absorptive enterocytes—is extremely short (3 to 5 days in mouse and human), with IECs being regenerated continuously from intestinal stem cells (ISCs) that reside in a region near the base of intestinal crypts (see Fig. S1 in the supplemental material) (1, 2). ISCs engage daily in self-renewal and generate highly proliferative progeny known as transient amplifying (TA) cells (1, 2). The nascent TA cells divide rapidly, migrate out of the stem cell niche, and initiate differentiation into the various cell lineages of mature intestinal villi, including absorptive enterocytes, mucin-producing goblet cells, peptide hormone–secreting enteroendocrine cells, and antimicrobial peptide-producing Paneth cells. Cells of the first three of these four lineages mature and migrate up the crypt toward the tip of intestinal villi, whereas Paneth cells travel down to the crypt bottom. Eventually, the mature cells die and are expelled from the luminal surface of the intestinal epithelium (1, 2). The elimination of older cells is thus balanced by the continuous production of new IECs in each crypt, resulting in a rapid turnover of IECs. Given that dysregulation of IEC elimination by cell death results in the development of intestinal inflammation (3, 4), the proper turnover of IECs is important for intestinal homeostasis. The specific molecular mechanisms underlying the regulation of IEC turnover remain poorly understood, however.

The continuous division of progenitor cells such as TA cells in the crypt is thought to exert a force that acts on the existing mature IECs and promotes their migration along the crypt-villus axis (5, 6). The proliferative activity of such crypt cells is thus likely a major determinant of the turnover rate of mature IECs. The Wnt–β-catenin signaling pathway plays an important role in the maintenance of ISCs as well as in the generation of Paneth cells, which contribute to the stem cell niche by secreting Wnt ligands such as Wnt3 (7). The Wnt signaling pathway is also implicated in positive regulation of TA cell proliferation (2, 8). The Notch signaling pathway is also thought to be important for maintenance of the ISC pool, and it contributes to regulation of the differentiation both of secretory cells such as goblet and Paneth cells and of absorptive enterocytes from progenitor cells (9, 10). Epidermal growth factor (EGF), whose receptor is a protein tyrosine kinase (PTK), is thought to serve as a major driver of TA cell proliferation through activation of the Ras–extracellular signal-regulated kinase (ERK) signaling pathway (2, 11). However, Ras was recently shown to promote the generation of both absorptive enterocytes and goblet cells by counteracting the Wnt signaling pathway, and it was unexpectedly found to be dispensable for the maintenance of ISCs and the proliferation of crypt cells (12, 13). EphB, another receptor-type PTK, has also been implicated in the proliferation of crypt cells (14).

Src family kinases (SFKs), including c-Src, Fyn, and c-Yes, are nonreceptor PTKs that play important roles in the regulation of cell proliferation, migration, and differentiation (15). The active forms of SFKs have been detected specifically in the crypt region of the intestinal epithelium (16). Whereas IEC-specific ablation of c-Src in mice resulted in no apparent defect, that of c-Src together

Received 31 May 2016 **Returned for modification** 21 June 2016
Accepted 18 August 2016

Accepted manuscript posted online 22 August 2016

Citation Imada S, Murata Y, Kotani T, Hatano M, Sun C, Konno T, Park J-H, Kitamura Y, Saito Y, Ohdan H, Matozaki T. 2016. Role of Src family kinases in regulation of intestinal epithelial homeostasis. Mol Cell Biol 36:2811–2823. doi:10.1128/MCB.00311-16.

Address correspondence to Yoji Murata, ymurata@med.kobe-u.ac.jp, or Takashi Matozaki, matozaki@med.kobe-u.ac.jp.

* Present address: Jung-ha Park, Department of Life Science and Biotechnology, College of Natural Sciences and Human Ecology, Dong-Eui University, Busan, Republic of Korea.

Supplemental material for this article may be found at http://dx.doi.org/10.1128/MCB.00311-16.

with Fyn and c-Yes led to an increase in the extent of IEC apoptosis in villi as well as a reduction in the number of Paneth cells in the small intestine under the steady-state condition (16). Moreover, IEC-specific ablation of c-Src alone prevented the regeneration of crypts after the induction of DNA damage by gamma irradiation (16). SFKs are thus likely important for the proliferation of IECs, in particular that of crypt cells, and for intestinal homeostasis. The precise role of SFKs in the regulation of IEC turnover and intestinal homeostasis, particularly in the steady-state condition, and the signaling pathways by which SFKs mediate such regulation remain unclear, however.

To address this issue, we have now generated and analyzed conditional knockout (CKO) mice in which COOH-terminal Src kinase (Csk) is genetically ablated specifically in IECs. Csk is a PTK that inhibits the activity of all SFKs by mediating their phosphorylation at a COOH-terminal regulatory tyrosine residue (Tyr^{527} in avian c-Src) (15, 17). Genetic ablation of Csk in mice was thus previously shown to result in hyperactivation not only of c-Src but also of other SFK members (18, 19). Given that c-Src as well as Fyn and c-Yes is expressed in the intestinal epithelium (16), we took advantage of this function of Csk to examine the role of SFKs in this tissue.

MATERIALS AND METHODS

Antibodies and reagents. Mouse monoclonal antibodies (MAbs) to β-catenin, to c-Yes, and to Rac1 were obtained from BD Biosciences (San Diego, CA), and those to phosphotyrosine (4G10) and to v-Src were from Merck Millipore (Darmstadt, Germany). A mouse MAb to β-tubulin and a rat MAb to bromodeoxyuridine (BrdU) were obtained from Sigma-Aldrich (St. Louis, MO) and Abcam (Cambridge, MA), respectively. Rabbit polyclonal antibodies (PAbs) to Csk, to Fyn, and to mucin 2 were obtained from Santa Cruz Biotechnology (Santa Cruz, CA). Rabbit PAbs to phospho-Tyr^{527} c-Src, to phospho-Tyr^{416} SFKs, to Yes-associated protein (YAP), to phospho-Ser^{127} YAP, to phospho-Ser^{381} YAP, to signal transducer and activator of transcription 3 (STAT3), to phospho-Tyr^{705} STAT3, to AKT, to phospho-Ser^{473} AKT, to ERK1/2, to phospho-Thr^{202}/Tyr^{204} ERK1/2, to cleaved caspase-3 (Asp^{175}), to focal adhesion kinase (FAK), to phospho-$Tyr^{576/577}$ FAK, to lamin A/C, and to Cre were obtained from Cell Signaling Technology (Beverly, MA). Rabbit PAbs to Ki67 were from Acris (Herford, Germany), those to human lysozyme were from Dako (Glostrup, Denmark), and those to phospho-Tyr^{357} YAP and to chromogranin A were from Abcam. A rat MAb to E-cadherin was obtained from TaKaRa (Kyoto, Japan). Horseradish peroxidase-conjugated goat secondary PAbs for immunoblot analysis were obtained from Jackson ImmunoResearch (West Grove, PA). Cy3- or Alexa Fluor 488-conjugated goat secondary PAbs for immunofluorescence analysis were obtained from Jackson ImmunoResearch and Invitrogen (Carlsbad, CA), respectively. 4′,6-Diamidino-2-phenylindole (DAPI) was obtained from Nacalai Tesque (Kyoto, Japan), and NSC23766 and verteporfin were from Santa Cruz Biotechnology and Sigma-Aldrich, respectively. Alex Fluor 488-conjugated cholera toxin B subunit was from Invitrogen. Mayer's hemalum solution, PP2, and PP3 was from Merck KGaA (Darmstadt, Germany), and eosin was from Wako (Osaka, Japan).

Mice. $Csk^{fl/fl}$ mice were kindly provided by M. Okada (20), and villin-*cre* mice [B6.SJL-Tg(Vil-cre)997Gum/J] were obtained from Jackson Laboratory (Bar Harbor, ME). Villin-*cre* mice were crossed with $Csk^{fl/fl}$ mice to generate $Csk^{fl/+}$; villin-*cre* offspring, which were then crossed with $Csk^{fl/fl}$ mice to obtain $Csk^{fl/fl}$; villin-*cre* (Csk CKO) and $Csk^{fl/fl}$ (control) animals. All mice were maintained at the Institute for Experimental Animals at Kobe University Graduate School of Medicine under specific-pathogen-free conditions. All animal experiments were performed according to Kobe University animal experimentation regulations.

Detection of deleted and floxed alleles of *Csk* by PCR. Various tissues of adult mice were washed with ice-cold phosphate-buffered saline (PBS), incubated overnight at 56°C in lysis buffer (100 mM Tris-HCl [pH 8.5], 5 mM EDTA, 0.2% sodium dodecyl sulfate [SDS], 200 mM NaCl, 50 μg/ml proteinase K), and centrifuged at 17,500 × *g* for 15 min at room temperature. The resulting supernatant was subjected to isopropanol precipitation for separation of genomic DNA. The floxed (~650-bp product) and deleted (~150-bp product) alleles of *Csk* were identified by PCR with the sense primer CskF (5′-TGGGGTTGAATGGTATGAACACTC-3′) and the antisense primer CskR (5′-TGCCATGTGGAGAAGAGAATCAGC-3′).

Isolation of IECs. Mouse IECs were isolated as previously described (21), with slight modifications. In brief, the freshly isolated ileum or colon of adult mice was washed with PBS, cut into small pieces, washed three times with Hanks' balanced salt solution (HBSS) containing 1% fetal bovine serum and 25 mM HEPES-NaOH (pH 7.5), and then incubated three or four times on a rolling platform for 15 min at room temperature in HBSS containing 5 mM EDTA and 25 mM HEPES-NaOH (pH 7.5). The tissue debris was removed, and IECs in the resulting supernatant were isolated by centrifugation at 500 × *g* for 10 min at 4°C and washed three times with PBS.

Immunoprecipitation and immunoblot analysis. Isolated IECs, tissues, or intestinal crypts or organoids were washed with ice-cold PBS and then homogenized on ice in radioimmunoprecipitation assay (RIPA) buffer (20 mM Tris-HCl [pH 7.5], 150 mM NaCl, 2 mM EDTA, 1% Nonidet P-40, 1% sodium deoxycholate, 0.1% SDS) containing 1 mM sodium vanadate, 50 mM NaF, and a protease inhibitor cocktail (Nacalai Tesque). The lysates were centrifuged at 17,500 × *g* for 30 min at 4°C, and the resulting supernatants were subjected to immunoprecipitation and immunoblot analysis as previously described (22).

Histology and immunofluorescence analysis. For histological analysis, the small intestine and colon were removed and immediately fixed for >12 h at room temperature with 4% paraformaldehyde in PBS. Paraffin-embedded sections (thickness of 5 μm) were then prepared and stained with hematoxylin-eosin. For immunofluorescence analysis, the small intestine or colon was fixed for 3 h at room temperature with 4% paraformaldehyde in PBS, transferred to a series of sucrose solutions (7, 20, and 30% [wt/vol], sequentially) in PBS for cryoprotection, embedded in optical cutting temperature (OCT) compound (Sakura, Tokyo, Japan), and rapidly frozen in liquid nitrogen. Frozen sections with a thickness of 5 μm were prepared with a cryostat, mounted on glass slides, and air dried. The sections were then stained with primary antibodies and fluorescent dye-labeled secondary antibodies as described previously (21). Images were obtained with a fluorescence microscope (BX51; Olympus, Tokyo, Japan) or a confocal laser scanning microscope (LSM710; Carl Zeiss, Oberkochen, Germany).

BrdU incorporation assay. Mice were injected intraperitoneally with BrdU (50 mg/kg) and killed 2, 24, or 72 h later. The ileum or colon was fixed with 4% paraformaldehyde, transferred to a series of sucrose solutions in PBS, embedded in OCT compound, and rapidly frozen with liquid nitrogen as described for immunofluorescence analysis. Sections with a thickness of 5 μm were incubated for 30 min at 65°C with 0.025 M HCl, washed with 0.1 M borate buffer (pH 8.5), and incubated at room temperature first for 2 h with antibodies to BrdU and to β-catenin and then for 1 h with fluorescent dye-labeled secondary antibodies. Fluorescence images were obtained with a fluorescence microscope (BX51; Olympus). The distances from the crypt base to the farthest-migrated BrdU-positive cells and to the villus tip were measured with the use of ImageJ software (NIH).

***In situ* hybridization.** Expression of *Olfm4* in the intestinal epithelium was examined by *in situ* hybridization performed as described previously (12). In brief, paraffin-embedded sections of the ileum (thickness of 10 μm) were depleted of paraffin with xylene, rehydrated by exposure to a graded series of ethanol solutions, and treated with 0.2 M HCl and proteinase K. The sections were then fixed again with 4% paraformaldehyde, demethylated with acetic anhydride, and subjected to hybridization

for 48 h at 65°C with a digoxigenin-labeled RNA probe for *Olfm4* mRNA (Image clone 1078130) at 500 ng/ml. They were then incubated overnight at 4°C with alkaline phosphatase-conjugated sheep PAbs to digoxigenin (Roche, Basel, Switzerland), washed, incubated with nitroblue tetrazolium chloride and 5-bromo-4-chloro-3-indolylphosphate (Sigma-Aldrich), and examined with a BX51 microscope (Olympus).

Isolation of mouse intestinal crypts and intestinal organoid culture. Crypts were isolated from the mouse small intestine and intestinal organoid culture was performed as described previously (12), with slight modifications. In brief, the small intestine was opened longitudinally and washed with ice-cold PBS. The villi were scraped from the mucosa with a cover glass during observation with a stereoscopic microscope (Olympus, Tokyo, Japan). The remaining tissue was then cut into pieces, washed with ice-cold PBS, incubated for 30 min in PBS containing 2 mM EDTA, and mixed vigorously for 30 s to release crypts. Tissue debris was removed, and crypts in the resulting supernatant were isolated by centrifugation at 300 × *g* for 5 min at 4°C. For intestinal organoid culture, isolated crypts were mixed with Matrigel (BD Biosciences) and transferred to 48-well plates. After polymerization of the Matrigel, advanced Dulbecco's modified Eagle's medium–F-12 (Invitrogen), which was supplemented with penicillin-streptomycin (100 U/ml) (Invitrogen), 10 mM HEPES (Invitrogen), 1× GlutaMAX (Invitrogen), 1× N2 (Invitrogen), 1× B27 (Invitrogen), 1.25 mM *N*-acetylcysteine (Sigma-Aldrich), 50 ng/ml EGF (Peprotech, Rocky Hill, NJ), 10% R-spondin1–Fc–conditioned medium, and 100 ng/ml Noggin (Peprotech), was overlaid on the gel in each well. The cultures were then maintained in an incubator (37°C, 5% CO_2). Phase-contrast images of intestinal organoids in Matrigel were obtained with an Axiovert 200 microscope (Carl Zeiss). For whole-mount immunofluorescence analysis, intestinal organoids in Matrigel were fixed with 4% paraformaldehyde and isolated from the gel with Cell Recovery Solution (BD Biosciences). The isolated organoids were then stained with primary antibodies and fluorescent dye-labeled secondary antibodies as well as with DAPI. Images were acquired with a confocal laser scanning microscope (LSM710, Carl Zeiss).

Isolation of RNA and quantitative RT-PCR analysis. Total RNA was isolated from IECs, intestinal crypts, or intestinal organoids with the use of an RNeasy minikit (Qiagen, Hilden, Germany), and portions (0.5 μg) of the RNA were subjected to reverse transcription (RT) with the use of a QuantiTect reverse transcription kit (Qiagen). The resulting cDNA was amplified by PCR with the use of Fast Start SYBR green Master (Roche, Penzberg, Germany) and a LightCycler 480 instrument (Roche). The amplification was analyzed with the use of LightCycler 480 software (Roche), and the abundance of each target mRNA was normalized by that of glyceraldehyde-3-phosphate dehydrogenase (GAPDH) mRNA. Primer sequences (forward and reverse, respectively) were as follows: *Olfm4*, 5′-TGGCCCTTGGAAGCTGTAGT-3′ and 5′-ACCTCCTTGGCCATAGCGAA-3′; *Lgr5*, 5′-ACCCGCCAGTCTCCTACATC-3′ and 5′-GCATCTAGGCGCAGGGATTG-3′; *Bmi1*, 5′-CCAATGAAGACCGAGGAGAA-3′ and 5′-TTTCCGATCCAATCTGCTCT-3′; *Hopx*, 5′-GAGGACCAGGTGGAGATCCT-3′ and 5′-TCCGTAACAGATCTGCATTCC-3′; *Ascl2*, 5′-CTACTCGTCGGAGGAAAG-3′ and 5′-ACTAGACAGCATGGGTAAG-3′; *Axin2*, 5′-GGACTGGGGAGCCTAAAGGT-3′ and 5′-AAGGAGGGACTCCATCTACGC-3′; *EphB2*, 5′-AGAATGGTGCCATCTTCCAG-3′ and 5′-GCACATCCACTTCTTCAGCA-3′; *EphB3*, 5′-CGTGAAAGTGGACACCATTG-3′ and 5′-CCAAGTAGAAGCCAGCCTTG-3′; *Yap*, 5′-CCCGACTCCTTCTTCAAGC-3′ and 5′-CTCGAACATGCTGTGGAGTC-3′; *Areg*, 5′-TCTGCCATCATCCTCGCAGCTATT-3′ and 5′-CGGTGTGGCTTGGCAATGATTCAA-3′; *Hes1*, 5′-GGACAAACCAAAGACGGCCTCTGAGCACAG-3′ and 5′-TGCCGGGAGCTATCTTTCTTAAGTGCATCC-3′; and GAPDH, 5′-AGGTCGGTGTGAACGGATTTG-3′ and 5′-TGTAGACCATGTAGTTGAGGTCA-3′.

Quantification of organoid area and bud formation in intestinal organoids. Intestinal organoids were cultured as described above and imaged with an Axiovert 200 microscope (Carl Zeiss). The organoid area was measured by outlining the periphery of each organoid with the use of ImageJ software. Any protrusions that contained Paneth cells were defined as buds, and their number per organoid was counted.

Assay of activated Rac. A glutathione *S*-transferase (GST) fusion protein (GST-CRIB) that contained the Cdc42- and Rac-interactive binding (CRIB) domain (amino acids 70 to 106) of rat p21PAKα was expressed in *Escherichia coli* and purified with the use of glutathione-Sepharose beads (GE Healthcare, Pittsburgh, PA) as previously described (22). Activated Rac was assayed as described previously (23). In brief, intestinal crypts were lysed in a solution containing 50 mM Tris-HCl (pH 7.4), 150 mM NaCl, 1% Nonidet P-40, 10 mM NaF, 1 mM EDTA, 1 mM EGTA, 1 mM phenylmethylsulfonyl fluoride, and aprotinin (10 μg/ml). The lysates were incubated for 60 min at 4°C with a GST-CRIB protein bound to glutathione-Sepharose beads. Proteins that bound to the beads were subjected to immunoblot analysis with antibodies to Rac1. The total abundance of Rac protein was also determined by immunoblot analysis of cell lysates.

Preparation of cytoplasmic and nuclear extracts. Cytoplasmic and nuclear extracts were prepared from crypts of mouse ileum with the use of the NE-PER reagent (Pierce, Rockford, IL).

Statistical analysis. Quantitative data are presented as means ± standard errors of the means (SEM) and were analyzed with Student's *t* test for comparisons between two groups or by one-way analysis of variance (ANOVA) followed by Tukey's *post hoc* test for comparisons among three or more groups. A *P* value of <0.05 was considered statistically significant. Analysis was performed with the use of GraphPad Prism software (GraphPad Software, La Jolla, CA).

RESULTS

Generation of IEC-specific Csk CKO mice. To investigate the role of SFKs in the regulation of intestinal epithelial homeostasis, we crossed mice homozygous for a floxed (fl) *Csk* allele (19, 20) with those harboring a transgene for Cre recombinase under the control of the villin gene promoter (villin-*cre*) (24). In adult $Csk^{fl/fl}$; villin-*cre* (Csk CKO) mice, Cre protein was specifically expressed in IECs throughout the intestinal crypts and villi, although its expression level was higher in IECs at villi than in crypt cells (see Fig. S2A in the supplemental material). The specificity and efficiency of *Csk* deletion in adult Csk CKO mice were determined by PCR analysis of genomic DNA isolated from the intestine and other organs. Consistent with the results of previous studies with the villin-*cre* transgene (12), deleted *Csk* alleles were detected in the small intestine (ileum) and colon of Csk CKO mice but not in other organs (see Fig. S2B). Immunoblot analysis also showed that the abundance of Csk protein in IECs isolated from the ileum or colon of Csk CKO mice was greatly reduced compared with that for $Csk^{fl/fl}$ (control) mice, whereas it was unaffected in other organs (Fig. 1A). The activation of SFKs is achieved by autophosphorylation (at Tyr^{416} in avian c-Src), whereas their inhibition is mediated by phosphorylation at the COOH-terminal regulatory Tyr residue (Tyr^{527} in avian c-Src) by Csk (15, 17). Phosphorylation of SFKs at the autophosphorylation site was markedly increased, whereas that at the COOH-terminal regulatory Tyr was abolished, in IECs from the ileum and colon of Csk CKO mice (Fig. 1B). These results thus indicated that the villin-*cre* transgene directed the efficient and specific deletion of *Csk* in IECs and that such deletion resulted in hyperactivation of SFKs in these cells.

Hyperplasia of the intestinal epithelium in Csk CKO mice. Csk CKO mice appeared healthy at birth, were born in the expected Mendelian ratio, and did not manifest any overt developmental defects (see Fig. S2C and D in the supplemental material). Histological examination of the small intestine and colon revealed no marked difference in crypt architecture or in villus or epithelial

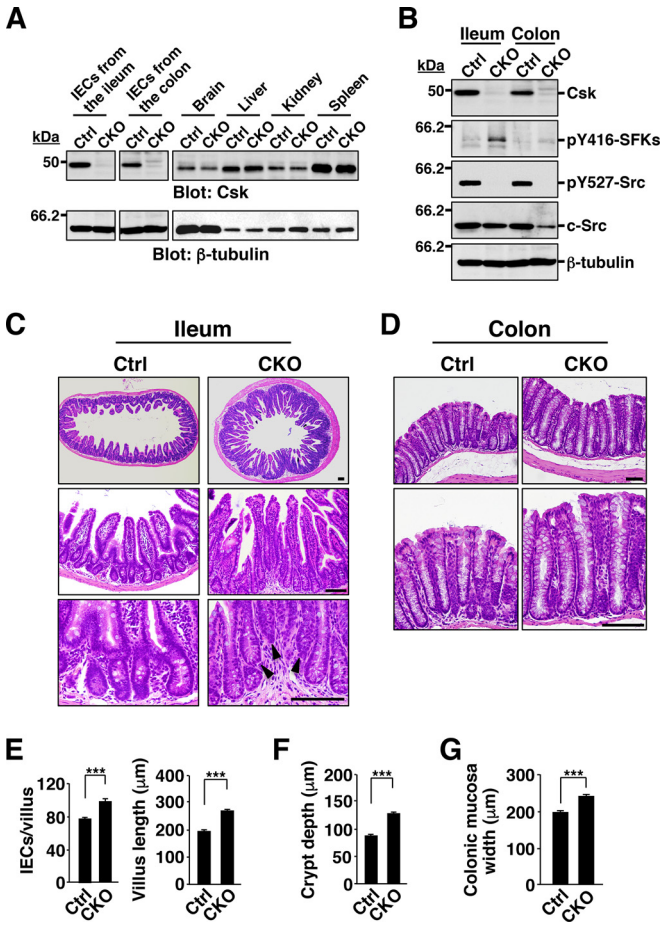

FIG 1 Hyperplasia of the intestinal epithelium in Csk CKO mice. (A) Lysates of IECs (from the ileum or colon) and of the indicated organs from 8-week-old control (Ctrl) or Csk CKO mice were subjected to immunoblot analysis with antibodies to Csk and to β-tubulin (loading control). (B) Lysates of IECs isolated from the ileum or colon of 8-week-old control or Csk CKO mice were subjected to immunoblot analysis with antibodies specific for Csk, for c-Src, or for the indicated phosphorylated (p) forms of Src family kinases. (C) Hematoxylin-eosin staining of paraffin-embedded sections of the ileum from control or Csk CKO mice at 40 weeks of age. Scale bars, 100 μm. Arrowheads indicate abnormally positioned crypts. (D) Hematoxylin-eosin staining of paraffin-embedded sections of the colon from control or Csk CKO mice at 40 weeks of age. Scale bars, 100 μm. (E) The number of IECs per villus (left panel) and villus length (right panel) as measured in sections similar to those in panel C. (F) Crypt depth measured in sections similar to those in panel C. (G) Width of the colonic mucosa measured in sections similar to those in panel D. Quantitative data are means ± SEM for 60 villi (E, left panel), 75 villi (E, right panel), 75 crypts (F), and 75 measurements (G) in a total of three mice of each genotype. ***, $P < 0.001$ (Student's t test). Immunoblots are representative of at least three separate experiments.

cell morphology between control and Csk CKO mice at 8 weeks of age (see Fig. S2E). In contrast, epithelial hyperplasia was found to be pronounced in the small intestine and colon of 40-week-old Csk CKO mice (Fig. 1C and D). Indeed, the number of IECs and the length of individual villi in the ileum were significantly increased for the mutant mice compared with control mice (Fig. 1E). The depth of crypts in the small intestine was also increased in the mutant animals (Fig. 1F). Moreover, whereas all crypts were positioned in a line in control mice, some crypts showed an abnormal shift toward the luminal side in the ileum of Csk CKO mice (Fig. 1C), suggesting that the increased proliferation of IECs resulted in the crowding of crypts. The width of the colonic mucosa in Csk CKO mice was also increased compared with that in control animals (Fig. 1G).

Increased proliferative activity of crypt IECs in Csk CKO mice. Given that SFKs play an important role in the regulation of cell proliferation and migration (15), we examined the incorporation of BrdU into IECs as well as the turnover of BrdU-labeled IECs in Csk CKO mice at 8 weeks of age. At 2 h after BrdU injection, the number of BrdU-positive IECs in crypts of the ileum (Fig. 2A) or colon (Fig. 2B) was markedly increased for Csk CKO mice compared with control mice. Immunostaining for Ki67, a marker of cell proliferation (25), also showed a marked increase in the number of Ki67-positive cells in crypts of the ileum of Csk CKO mice (Fig. 2C). ISCs and TA cells constitute the majority of proliferative cells in crypts. *In situ* hybridization revealed that the number of *Olfm4* mRNA-positive cells, which likely correspond to ISCs (26), at the crypt base was markedly reduced in the ileum of Csk CKO mice at 8 weeks of age (Fig. 2D). Consistent with this result, RT-PCR analysis revealed that the abundance of mRNAs for the ISC marker proteins Olfm4, Lgr5, Bmi1, and Hopx (1) was significantly reduced in crypts isolated from the small intestine of Csk CKO mice at 8 weeks of age (Fig. 2E). Wnt–β-catenin signaling is thought to play a key role in the maintenance of ISCs and the proliferation of their progeny (1, 2, 8). Expression of the Wnt–β-catenin target gene *Axin2* was significantly reduced, whereas that of *Ascl2* and *EphB2*, which are also Wnt–β-catenin target genes, tended to be reduced, in crypts isolated from the ileum of Csk CKO mice compared with those isolated from control mice (Fig. 2E). These results suggested that SFKs promote the proliferative activity of crypt cells such as TA cells. In contrast, SFKs likely suppress the Wnt–β-catenin signaling pathway and reduce the population of ISCs in the crypts. We further investigated whether the reduction in the number of *Olfm4* mRNA–positive cells in Csk CKO mice is attributable to apoptosis. The number of cells positive for the cleaved form of caspase-3 in crypts or villi of the ileum did not differ significantly between Csk CKO and control mice (see Fig. S3A in the supplemental material), suggesting that the reduction in the number of ISCs at the crypt base of Csk CKO mice is not likely due to increased apoptosis.

We also found that at 1 day after BrdU injection, whereas most BrdU-positive IECs remained in a position immediately above or within crypt areas of the ileum in control mice, most such cells in the ileum of Csk CKO mice had migrated to the middle region or tip of villi (Fig. 3A). Quantitative analysis confirmed that the migration distance of BrdU-labeled IECs in the ileum was markedly increased for Csk CKO mice (Fig. 3B). At 3 days after BrdU injection, BrdU staining in villi of the ileum in Csk CKO mice was greatly reduced compared with that apparent for control mice (Fig. 3C). These results suggested that both the migration of IECs along the crypt-villus axis and the turnover of mature IECs were markedly increased in the ileum of Csk CKO mice.

Aberrant localization of Paneth cells and increased number of goblet cells in Csk CKO mice. We next investigated whether IEC-specific ablation of Csk affects the numbers of Paneth cells, goblet cells, or enteroendocrine cells in the intestinal epithelium. The number of Paneth cells, which were stained with antibodies to lysozyme (21), was significantly reduced at the base of crypts in the ileum of Csk CKO mice at 8 weeks of age (Fig. 3D and E). Moreover, these cells were frequently localized outside the crypts in the

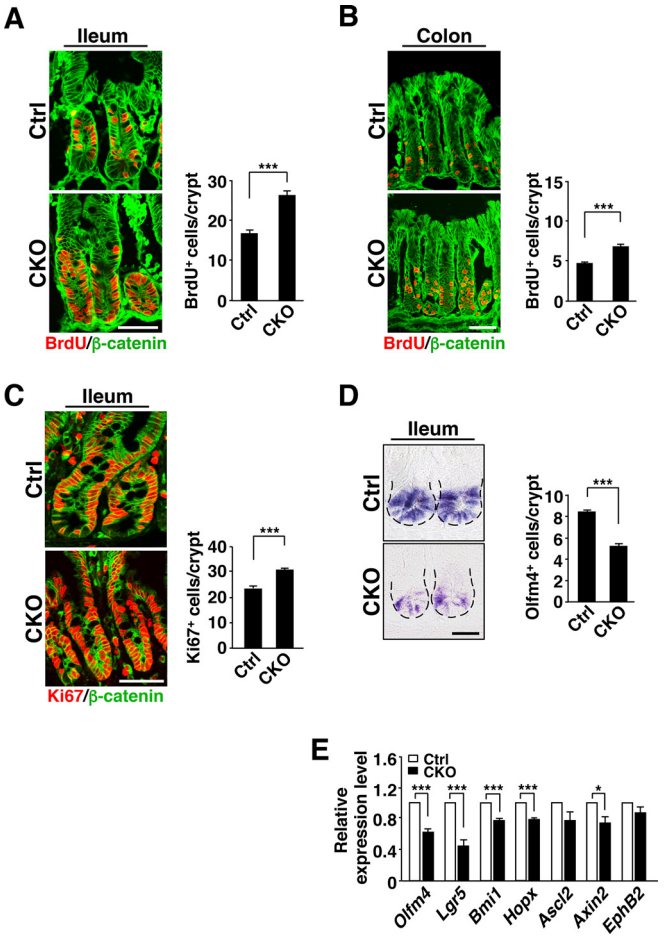

FIG 2 Increased proliferative activity of IECs in crypts of Csk CKO mice. (A) Frozen sections prepared from the ileum of 8-week-old control or Csk CKO mice at 2 h after BrdU injection were immunostained with antibodies to BrdU (red) and to β-catenin (green) (left panel). Scale bar, 50 μm. The number of BrdU-positive cells per crypt in such sections was also determined (right panel). (B) Frozen sections prepared from the colon of 8-week-old control or Csk CKO mice at 2 h after BrdU injection were immunostained, and the number of BrdU-positive cells per crypt was determined, as for panel A. Scale bar, 50 μm. (C) Frozen sections of the ileum from 8-week-old control or Csk CKO mice were immunostained with antibodies to Ki67 (red) and to β-catenin (green) (left panel). Scale bar, 50 μm. The number of Ki67-positive cells per crypt in such sections was also determined (right panel). (D) Paraffin-embedded sections of the ileum from 8-week-old control or Csk CKO mice were subjected to *in situ* hybridization analysis of *Olfm4* mRNA (left panel). Dashed lines indicate the base of the crypt epithelium. Scale bar, 25 μm. The number of *Olfm4* mRNA-positive (Olfm4$^+$) cells per crypt in such sections was also determined (right panel). (E) Quantitative RT-PCR analysis of ISC marker gene (*Olfm4*, *Lgr5*, *Bmi1*, and *Hopx*) and Wnt–β-catenin target gene (*Lgr5*, *Ascl2*, *Axin2*, and *EphB2*) expression in crypts isolated from the small intestine of 8-week-old control or Csk CKO mice. The amount of each mRNA was normalized by that of GAPDH mRNA and then expressed relative to the normalized value for control mice. Quantitative data are means ± SEM for 60 (A to C) or 90 (D) crypts from a total of three mice per genotype or for five separate experiments (E). *, $P < 0.05$; ***, $P < 0.001$ (Student's *t* test).

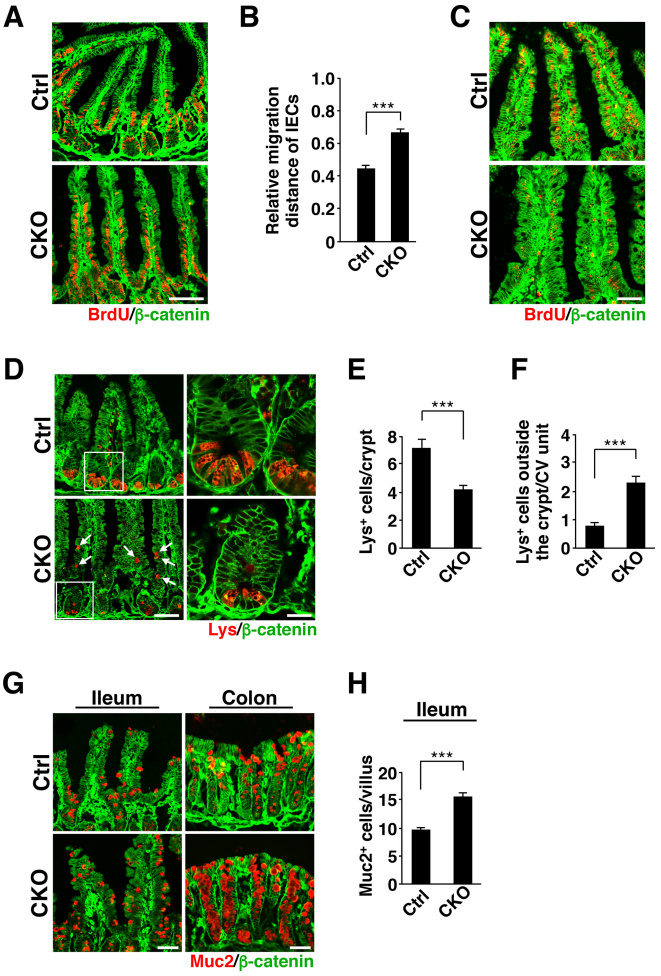

FIG 3 Increased migration and turnover of IECs, aberrant localization of Paneth cells, and increased number of goblet cells in Csk CKO mice. (A) Frozen sections prepared from the ileum of 8-week-old control or Csk CKO mice at 1 day after BrdU injection were subjected to immunostaining with antibodies to BrdU (red) and to β-catenin (green). Scale bar, 100 μm. (B) The distance from the crypt base to the farthest-migrated BrdU-positive cells as a proportion of that from the crypt base to the tip of the villus was measured in sections similar to those in panel A. (C) Frozen sections prepared from the ileum of 8-week-old control or Csk CKO mice at 3 days after BrdU injection were immunostained as for panel A. Scale bar, 50 μm. (D) Frozen sections of the ileum from 8-week-old control or Csk CKO mice were subjected to immunostaining with antibodies to lysozyme (Lys) (red) and to β-catenin (green). Boxed regions in the left images are shown at higher magnification in the right images. Arrows indicate Paneth cells mislocalized outside crypts. Scale bars, 100 μm (left images) and 20 μm (right images). (E) The number of lysozyme-positive (Lys$^+$) Paneth cells per crypt was determined for sections similar to those in panel D. (F) The number of lysozyme-positive Paneth cells located outside the crypt per crypt-villus (CV) unit was determined for sections similar to those in panel D. (G) Frozen sections of the ileum or colon from 8-week-old control or Csk CKO mice were immunostained with antibodies to mucin 2 (Muc2) (red) and to β-catenin (green). Scale bars, 50 μm. (H) The number of mucin 2-positive (Muc2$^+$) cells per villus of the ileum was determined for sections similar to those in panel G. Quantitative data are means ± SEM for 60 villi (B and F), 60 crypts (E), or 56 (control) or 58 (Csk CKO) villi (H) from a total of three mice per genotype. ***, $P < 0.001$ (Student's *t* test).

mutant animals (Fig. 3D). Indeed, the number of Paneth cells localized outside crypts was significantly increased in the ileum of Csk CKO mice compared with control mice (Fig. 3F). In addition, the level of mRNA for EphB3, which plays an important role in positioning of Paneth cells (27), tended to be reduced in crypts of Csk CKO mice (see Fig. S4A in the supplemental material). Conversely, the number of mucin 2-positive goblet cells was increased in the ileum and colon of Csk CKO mice (Fig. 3G and H). Ablation of Csk had no effect on the number of chromogranin A-positive enteroendocrine cells in the ileum (see Fig. S3B in the supplemen-

tal material). These results thus suggested that SFKs are important for regulation of both the number and positioning of Paneth cells in the small intestine and that they positively regulate the size of the goblet cell population.

Increased proliferative activity of IECs in intestinal organoids from Csk CKO mice. To clarify further the role of SFKs in IEC proliferation and differentiation in the intestinal epithelium, we examined the effects of Csk ablation on IECs in intestinal organoids. Intestinal crypts isolated from control or Csk CKO mice were thus cultured in medium containing EGF, R-spondin1, and Noggin to allow the formation of organoids (11, 12). Isolated crypts from control mice gradually developed into crypt-villus organoids, having formed several buds that correspond to crypts by 5 days after plating (Fig. 4A to C). The surface area of Csk-deficient intestinal organoids was much greater than that of control organoids for up to 2 days after plating (Fig. 4A and B). In addition, whereas Ki67 expression was restricted to buds in control organoids at 2 days after plating, it had spread throughout the Csk-deficient organoids at this time, resulting in a significant percent increase in the Ki67-positive area (Fig. 4D). In contrast, such an increased percentage of the Ki67-positive area of Csk-deficient organoids was markedly reduced by treatment with the SFK inhibitor PP2 (28) but not with PP3 (an inactive analogue of PP2) and vehicle (see Fig. S5 in the supplemental material), suggesting that the proliferative activity of IECs is increased in Csk-deficient organoids and that this increased activity is attributable to constitutive activation of SFKs. In addition, the number of Paneth cells in buds was markedly reduced (Fig. 4E), whereas that of goblet cells was increased (Fig. 4F), in the Csk-deficient organoids compared with control organoids at 3 days after plating. The amounts of *Olfm4*, *Lgr5*, and *Ascl2* mRNAs also tended to be reduced in the Csk-deficient organoids at 4 days after plating (*Olfm4* mRNA, $P = 0.31$ versus control; *Lgr5* mRNA, $P = 0.06$ versus control; *Ascl2* mRNA, $P = 0.24$ versus control) (Fig. 4G). These results suggested that the phenotypes of Csk-deficient organoids correspond well to those of the intestinal epithelium in Csk CKO mice. Furthermore, the phenotypes of IECs observed in Csk CKO mice are likely attributable to cell-autonomous effects of Csk ablation. The surface area of Csk-deficient intestinal organoids had become smaller than that of control organoids at day 5 (Fig. 4A and B), at which time the number of buds was also reduced for the organoids from Csk CKO mice (Fig. 4A and C).

Increased protein tyrosine phosphorylation and Rac activity in crypts of Csk CKO mice. We next investigated the molecular mechanism by which SFKs regulate IEC proliferation and differentiation in the intestinal epithelium. To this end, we first examined the localization of SFKs in the intestinal epithelium. Immunohistofluorescence analysis with antibodies to c-Src, to Fyn, or to c-Yes revealed that staining for these three SFKs was prominent along the apical surface of IECs in crypts, whereas it was less intense in other areas of the intestinal epithelium (Fig. 5A; see Fig. S6A in the supplemental material). The SFKs manifested a similar localization in crypts of Csk CKO mice (Fig. 5A; see Fig. S6A). Moreover, staining of the ganglioside GM1 as a marker for lipid rafts (29, 30) with the B subunit of cholera toxin revealed a pattern similar to that apparent for the three SFKs in intestinal crypts (see Fig. S6B). These results thus suggested that SFKs are likely localized in lipid rafts at the apical surface of IECs. We next subjected sections of the ileum to immunohistofluorescence staining with antibodies to phosphotyrosine. Whereas staining for phosphotyrosine was relatively weak throughout the intestinal crypts and villi of control mice, it was prominent in crypts of Csk CKO mice, especially along the apical surface of IECs (Fig. 5B). Moreover, a similar staining pattern was observed with antibodies to auto-

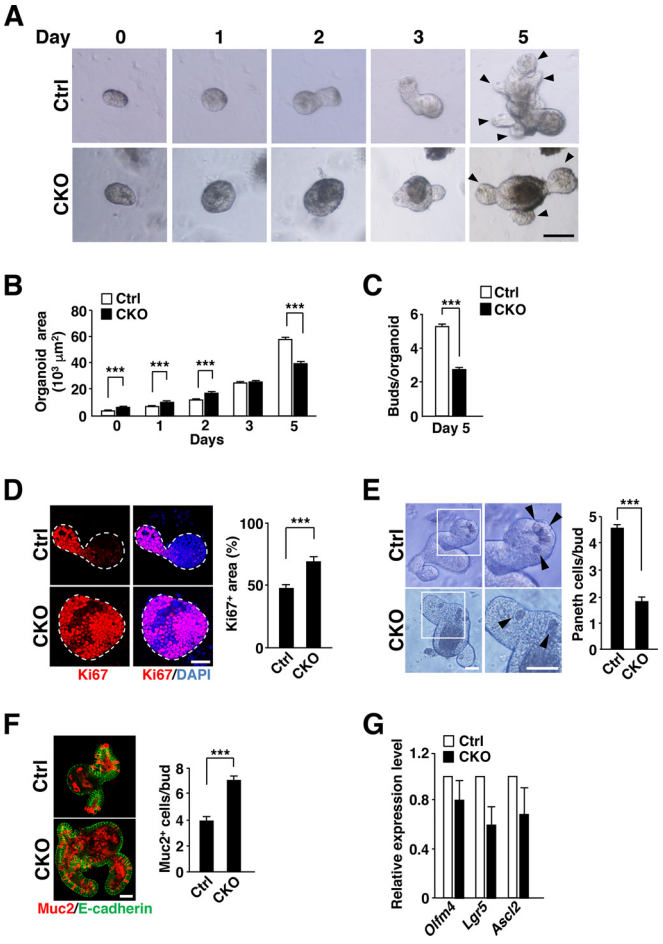

FIG 4 Increased proliferative activity of IECs in intestinal organoids from Csk CKO mice. (A) Intestinal organoids derived from the jejunum of 8-week-old control or Csk CKO mice were cultured for the indicated times and then examined by light microscopy. Arrowheads indicate cryptlike buds. Scale bar, 100 μm. (B) Area of intestinal organoids cultured as for panel A. (C) Number of buds per organoid for intestinal organoids cultured for 5 days as for panel A. (D) Intestinal organoids cultured for 2 days as for panel A were subjected to immunostaining with antibodies to Ki67 (red) as well as to staining of nuclei with 4′,6-diamidino-2-phenylindole (DAPI) (blue) (left panel). Dashed lines indicate the boundary of intestinal organoids. Scale bar, 100 μm. The Ki67-positive area as a percentage of the total area of each organoid was determined in such images with ImageJ software (right panel). (E) Intestinal organoids were cultured for 3 days as for panel A and then photographed (left panel). Boxed regions in the left images are shown at higher magnification in the right images. Arrowheads indicate granule-containing Paneth cells. Scale bars, 50 μm. The number of granule-containing Paneth cells per bud in such images was also determined (right panel). (F) Intestinal organoids cultured for 3 days as for panel A were subjected to immunostaining with antibodies to mucin 2 (red) and to E-cadherin (green) (left panel). Scale bar, 50 μm. The number of mucin 2-positive cells per bud in such sections was also determined (right panel). (G) Quantitative RT-PCR analysis of *Olfm4*, *Lgr5*, and *Ascl2* mRNAs in intestinal organoids cultured for 4 days as for panel A. The amount of each mRNA was normalized by that of GAPDH mRNA and then expressed relative to the normalized value for control organoids. Quantitative data are means ± SEM for a total of 75 organoids (B and D), 60 organoids (C), 60 buds (E), or 45 buds (F) per group in three separate experiments or for three separate experiments (G). ***, $P < 0.001$ (Student's *t* test).

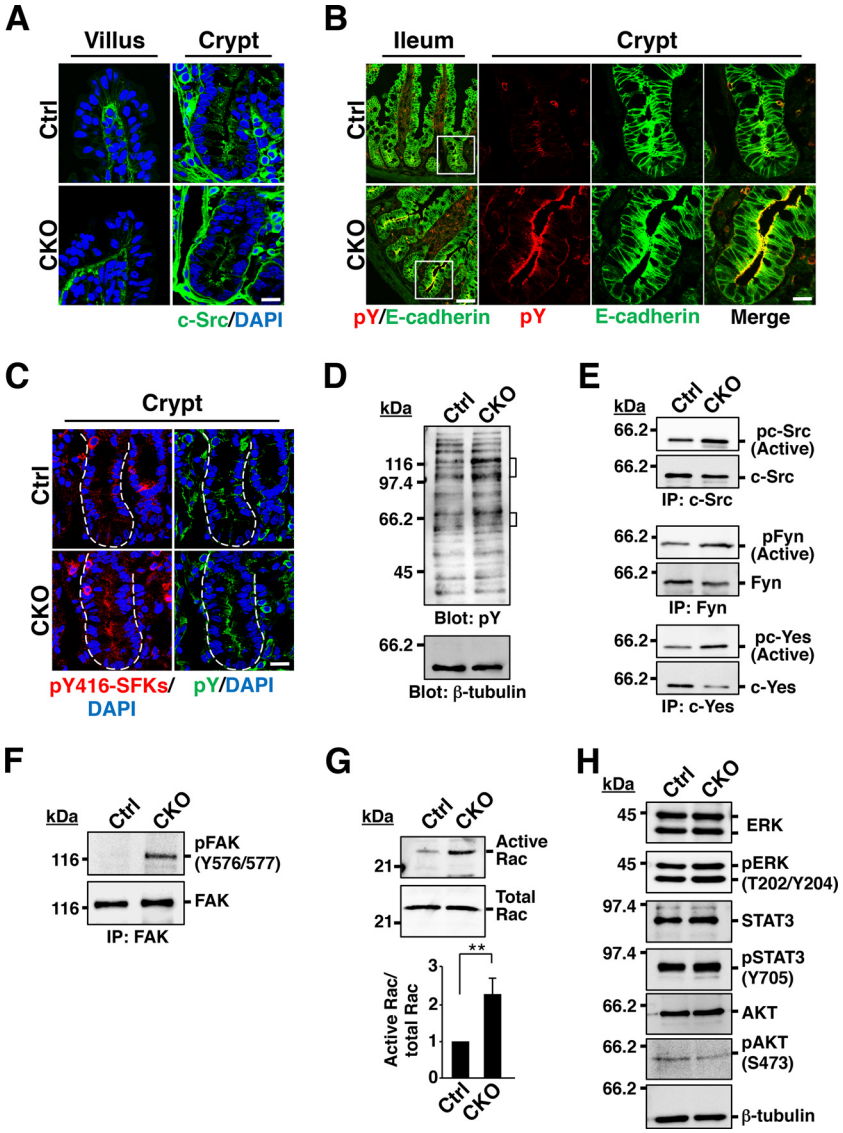

FIG 5 Increased protein tyrosine phosphorylation and Rac activity in crypts of Csk CKO mice. (A) Frozen sections of the ileum from 8-week-old control or Csk CKO mice were subjected to immunostaining with antibodies specific for c-Src (green) and to staining of nuclei with DAPI (blue). Scale bar, 20 μm. (B) Frozen sections of the ileum from 8-week-old control or Csk CKO mice were subjected to immunostaining with antibodies to E-cadherin (green) and to phosphotyrosine (pY) (red). Boxed regions in the left images (ileum) are shown at higher magnification in the right images (crypt). Scale bars, 50 μm (left images) and 20 μm (right images). (C) Frozen sections of the ileum from 8-week-old control or Csk CKO mice were subjected to immunostaining with antibodies specific for autophosphorylated SFKs (pY416-SFKs) (red) or for phosphotyrosine (green). Nuclei were also stained with DAPI (blue). Dashed lines indicate the base of the crypt epithelium. Scale bar, 20 μm. (D) Lysates of crypts isolated from the ileum of 8-week-old control or Csk CKO mice were subjected to immunoblot analysis with antibodies to phosphotyrosine and to β-tubulin. Brackets indicate proteins whose level of tyrosine phosphorylation was markedly increased in Csk CKO mice. (E) Crypts isolated from the ileum of 8-week-old control or Csk CKO mice were lysed and subjected to immunoprecipitation (IP) with antibodies to the indicated SFKs, and the resulting precipitates were subjected to immunoblot analysis with antibodies to autophosphorylated or total forms of the corresponding kinases. (F) Crypts isolated from the ileum of 8-week-old control or Csk CKO mice were lysed and subjected to immunoprecipitation with antibodies to FAK, and the resulting precipitates were subjected to immunoblot analysis with the same antibodies and antibodies to $Tyr^{576/577}$-phosphorylated FAK. (G) Crypts from the ileum of 8-week-old control or Csk CKO mice were lysed, and the GTP-bound (active) form of Rac was precipitated with a GST fusion protein containing the CRIB domain of p21PAKα. The resulting precipitates were subjected to immunoblot analysis with antibodies to Rac (upper panel). The lysates were also subjected directly to immunoblot analysis with the same antibodies to determine the total amount of Rac (middle panel). Immunoblots were subjected to densitometric analysis, and the ratio of the band intensity for GST-PAK-bound Rac (active Rac) to that for total Rac was calculated (lower panel). Quantitative data are expressed relative to the value for crypts of control mice and are means ± SEM from three independent experiments. **, $P < 0.01$ (Student's *t* test). (H) Crypts isolated from the ileum of 8-week-old control or Csk CKO mice were subjected to immunoblot analysis with antibodies to total or phosphorylated forms of the indicated signaling proteins.

phosphorylated SFKs (Fig. 5C; see Fig. S6C), suggesting that tyrosine phosphorylation of SFKs accounts, at least in part, for the increased phosphotyrosine content in crypts of Csk CKO mice. Immunoblot analysis with antibodies to phosphotyrosine showed that the extent of tyrosine phosphorylation of several proteins (molecular sizes of ~50 to 65 and ~100 to 120 kDa) was markedly increased in crypts isolated from the ileum of Csk CKO mice (Fig. 5D), with the group of smaller tyrosine-phosphorylated proteins

likely corresponding to SFKs. Indeed, immunoprecipitation and immunoblot analysis revealed that the tyrosine phosphorylation of c-Src as well as that of Fyn and c-Yes was increased in crypts isolated from the ileum of Csk CKO mice (Fig. 5E). With regard to the identity of the group of larger tyrosine-phosphorylated proteins, we found that phosphorylation of FAK, in particular at Tyr^{576} or Tyr^{577}, was markedly increased in crypts from Csk CKO mice (Fig. 5F). Given that phosphorylation of FAK at Tyr^{576} or Tyr^{577} by c-Src is thought to promote the activation of FAK (31), ablation of Csk in IECs likely results in FAK activation.

Activation of FAK by c-Src in response to ligation of integrins or growth factor stimulation is thought to result in activation of Rho family GTPases such as Rac (32, 33). Indeed, a pulldown assay performed with GST-tagged PAK, which binds the active form of Rac, showed that the activity of Rac in isolated crypts was significantly greater for Csk CKO mice than for control mice (Fig. 5G). Activation of ERK, STAT3, and the protein kinase AKT is also thought to be important for signaling downstream of SFKs (32, 34, 35). However, the phosphorylation levels of these signaling molecules were similar in crypts from control or Csk CKO mice (Fig. 5H).

Effects of a Rac inhibitor on the phenotypes of Csk-deficient intestinal organoids. Immunoblot analysis revealed that tyrosine phosphorylation of SFKs at the autophosphorylation site as well as phosphorylation of FAK at Tyr^{576} or Tyr^{577} was markedly increased in intestinal organoids from Csk CKO mice compared with those from control mice (Fig. 6A). Csk-deficient organoids thus appeared to recapitulate the signaling properties of the intestinal epithelium in Csk CKO mice. To investigate whether the phenotypes of Csk-deficient intestinal organoids are attributable to the upregulation of Rac activity, we examined the effects of the Rac inhibitor NSC23766 (36). This agent significantly attenuated the increase in the Ki67-positive area apparent in Csk-deficient organoids (Fig. 6B). In addition, it rescued in part the reduction in the number of Paneth cells in buds (Fig. 6C) and prevented the increase in the size of the goblet cell population (Fig. 6D) characteristic of these organoids. The tendency for the expression levels of *Olfm4*, *Lgr5*, and *Ascl2* to be reduced in Csk-deficient organoids was also no longer apparent in the presence of the Rac inhibitor (Fig. 6E). In contrast, treatment of control intestinal organoids with NSC23766 slightly prevented the development of organoids (see Fig. S7 in the supplemental material). Together, these results suggested that the increased proliferative activity as well as the altered populations of secretory cells in Csk-deficient organoids was attributable to hyperactivation of Rac. Both the reduction in the surface area and the defect in bud formation apparent in Csk-deficient organoids at 5 days after plating were also abolished by treatment with NSC23766 (Fig. 6F).

Importance of YAP for hyperproliferation of IECs in intestinal crypts of Csk CKO mice. YAP and TAZ function as transcriptional coactivators in the Hippo signaling pathway, with YAP being thought to promote cell proliferation and differentiation by regulating the expression of its target genes in various cell types, including IECs (37, 38). Activation of the Hippo signaling pathway upstream of YAP results in the degradation of YAP in the cytoplasm in a manner dependent on the ubiquitin-proteasome system. Conversely, inactivation of the Hippo pathway prevents the degradation of YAP, which then translocates to the nucleus and initiates transcription of its target genes (37). The amount of YAP in isolated crypts of the ileum was markedly greater for those from Csk CKO mice than for those from control mice (Fig. 7A), whereas the abundance of *Yap* mRNA in crypts did not differ between the two genotypes (see Fig. S8A in the supplemental material). Immunofluorescence analysis of the ileum revealed that YAP immunoreactivity was increased in crypt IECs of Csk CKO mice, with this increase being especially apparent in the cytoplasm (Fig. 7B). The phosphorylation of YAP at Ser^{381} by Lats is thought to promote the degradation of YAP in the cytoplasm and thereby to regulate the amount of this protein in cells (37, 39). In contrast, phosphorylation of YAP at Ser^{127} by Lats promotes the association of YAP with 14-3-3 and thereby prevents the nuclear translocation of YAP (37, 40). The level of YAP phosphorylation at both Ser^{127} and Ser^{381} was markedly reduced in crypts of Csk CKO mice compared with those of control mice (Fig. 7C). In addition, subcellular fractionation revealed that the amount of YAP was increased in both the cytoplasm and nucleus of crypts from Csk CKO mice (Fig. 7D). The expression of the YAP target gene for amphiregulin (*Areg*) (41, 42) was also significantly increased in crypts of the mutant mice (Fig. 7E). These results thus suggested that YAP-mediated signaling is activated by ablation of Csk in crypt IECs. We also confirmed that the abundance of YAP was increased in Csk-deficient organoids compared with control organoids (Fig. 7F). Strong staining for YAP was observed in IECs, particularly the nuclear region, of Csk-deficient organoids (Fig. 7G). Furthermore, this increase in YAP expression in the mutant organoids was significantly attenuated by treatment with the Rac inhibitor NSC23766 (Fig. 7H), suggesting that hyperactivation of Rac contributes to the upregulation of YAP abundance in Csk-deficient organoids.

Finally, to investigate further the role of YAP in the hyperproliferation of IECs and secretory cell imbalance in Csk CKO mice, we examined the effects of the YAP inhibitor verteporfin (43) on Csk-deficient organoids. Verteporfin significantly attenuated the expansion of the Ki67-positive area in Csk-deficient organoids, limiting the region of Ki67 staining to each cryptlike structure (Fig. 8A). It also suppressed the increase in the size of the goblet cell population (Fig. 8B) without affecting the reduction in the number of Paneth cells (Fig. 8C) apparent at the buds of Csk-deficient organoids. The reduction in the surface area and the defect in bud formation apparent for Csk-deficient organoids at 5 days after plating were both rescued by treatment with verteporfin (Fig. 8D).

DISCUSSION

We have here shown that Csk CKO mice, in which the activity of SFKs is likely elevated specifically in IECs, develop intestinal and colonic epithelial hyperplasia. The proliferative activity of IECs was markedly increased in crypts of the small intestine of Csk CKO mice as well as in intestinal organoids derived from these animals. In contrast, the number of ISCs in crypts was greatly reduced in the mutant mice. Given that TA cells and ISCs are the major cell types that manifest active proliferation in crypts, our results suggest that SFKs promote the proliferative activity of TA cells in the intestinal epithelium. In addition, the migration of BrdU-labeled IECs along the crypt-villus axis in the small intestine was faster for Csk CKO mice than for control mice, suggesting that SFKs promote IEC turnover, likely by stimulating the proliferation of TA cells, under the steady-state condition.

We also found that IEC-specific ablation of Csk resulted in a reduction in the number of Paneth cells at the base of crypts in the

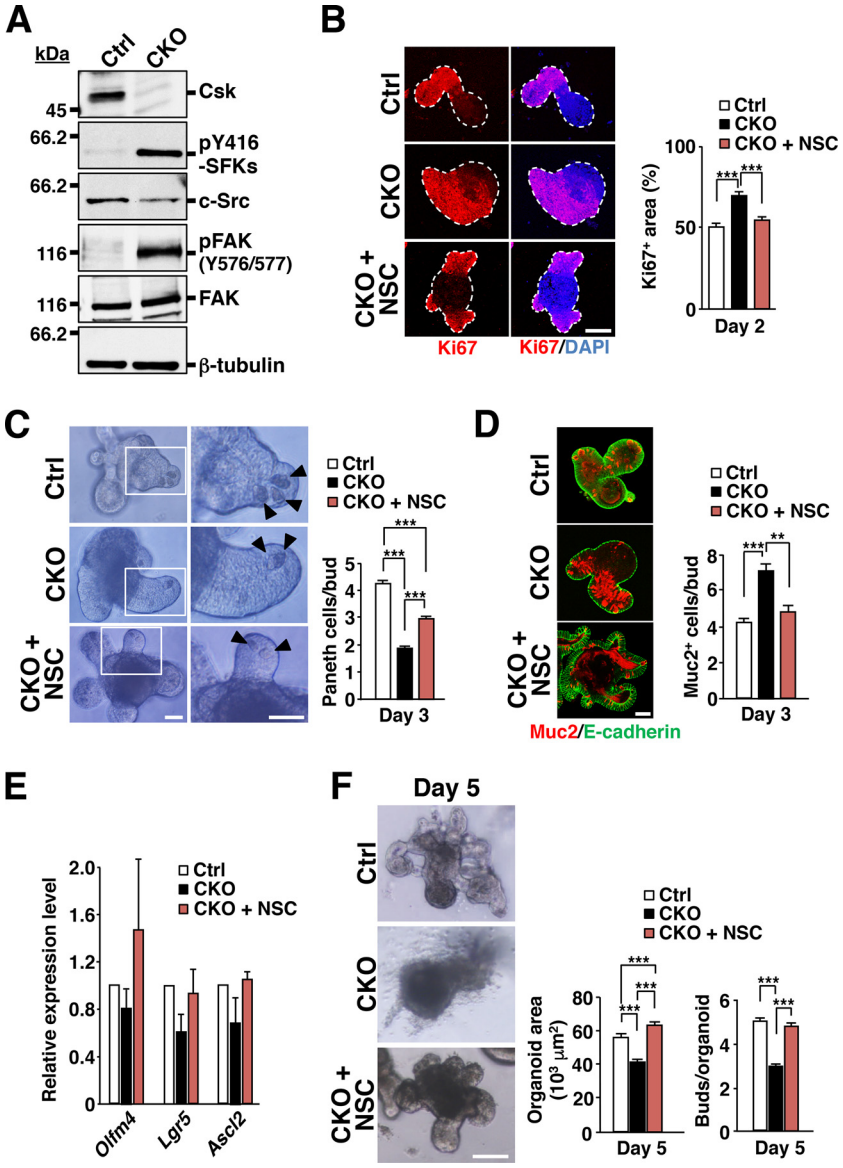

FIG 6 Effects of a Rac inhibitor on the phenotypes of Csk-deficient intestinal organoids. (A) Lysates of intestinal organoids derived from the jejunum of 8-week-old control or Csk CKO mice at 2 days after plating were subjected to immunoblot analysis with antibodies specific for the indicated proteins. (B) Intestinal organoids prepared as for panel A were cultured in the absence or presence of the Rac inhibitor NSC23766 (NSC) (50 μM) for 2 days and then subjected to immunostaining with antibodies to Ki67 (red) and to staining of nuclei with DAPI (blue) (left panel). Dashed lines indicate the boundary of intestinal organoids. Scale bar, 100 μm. The Ki67-positive area was also determined as a percentage of the total organoid area in such images (right panel). (C) Intestinal organoids cultured for 3 days as for panel B were examined by light microscopy (left panel). Boxed regions in the left images are shown at higher magnification in the right images. Arrowheads indicate granule-containing Paneth cells. Scale bars, 50 μm. The number of granule-containing Paneth cells per bud was also determined in such images (right panel). (D) Intestinal organoids cultured for 3 days as for panel B were subjected to immunostaining with antibodies to mucin 2 (red) and to E-cadherin (green) (left panel). Scale bar, 50 μm. The number of mucin 2-positive cells per bud was also determined in such images (right panel). (E) Quantitative RT-PCR analysis of *Olfm4*, *Lgr5*, and *Ascl2* mRNAs in intestinal organoids cultured for 4 days as for panel B. The amount of each mRNA was normalized by that of GAPDH mRNA and then expressed relative to the normalized value for control organoids. (F) Intestinal organoids cultured for 5 days as for panel B were examined by light microscopy (left panel). Scale bar, 100 μm. The organoid area (middle panel) and the number of buds per organoid (right panel) were also determined from such images. Quantitative data are means ± SEM for a total of 75 organoids (B and F [middle panel]), 60 buds (C), 45 buds (D), or 60 organoids (F [right panel]) per group in three separate experiments or for three separate experiments (E). **, $P < 0.01$; ***, $P < 0.001$ (ANOVA and Tukey's test).

small intestine. In contrast, it resulted in a marked increase in the number of goblet cells in villi of the small intestine as well as the colon. These phenotypes were also apparent in Csk-deficient intestinal organoids, suggesting that the characteristics of IECs observed in Csk CKO mice are likely attributable to cell-autonomous effects of Csk ablation. Given that TA cells are thought to give rise to these secretory cell types (1, 2), SFKs are likely important not only for the rapid division of TA cells but also for their differentiation into mature secretory cells, including Paneth and goblet cells. Consistent with this notion, we found that the active forms

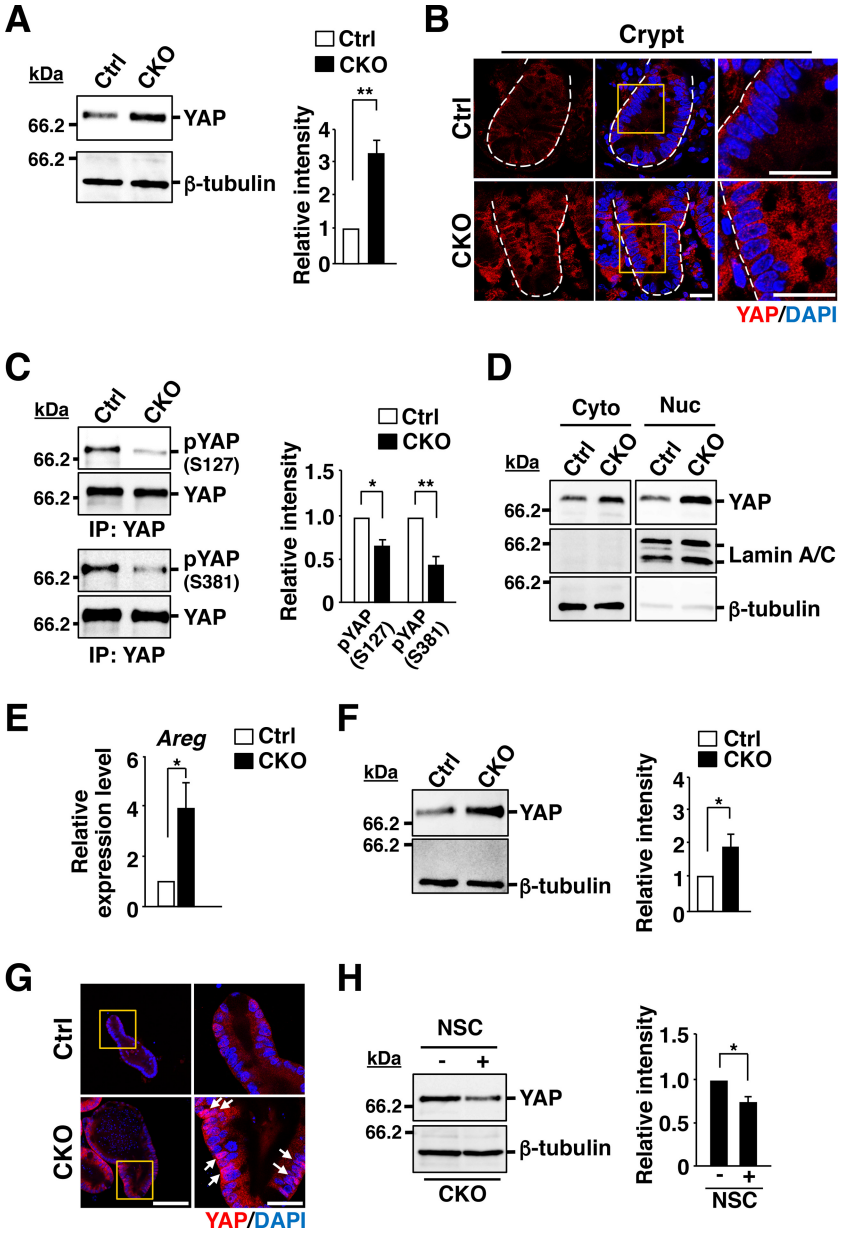

FIG 7 Upregulation of YAP abundance and activity in crypts of Csk CKO mice. (A) Lysates of crypts isolated from the ileum of 8-week-old control or Csk CKO mice were subjected to immunoblot analysis with antibodies to YAP and to β-tubulin (left panel). The band intensity for YAP in such blots was also normalized by that for β-tubulin and expressed relative to the normalized value for the crypts of control mice (right panel). (B) Frozen sections of the ileum from 8-week-old control or Csk CKO mice were subjected to immunostaining with antibodies to YAP (red) and to staining of nuclei with DAPI (blue). Boxed regions in the middle images are shown at higher magnification in the right images. Dashed lines indicate the base of the crypt epithelium. Scale bars, 20 μm. (C) Lysates of crypts from the ileum of 8-week-old control or Csk CKO mice were subjected to immunoprecipitation (IP) with antibodies to YAP, and the resulting precipitates were subjected to immunoblot analysis with the same antibodies as well as with antibodies to Ser^{127}- or Ser^{381}-phosphorylated YAP. The ratio of the band intensity for each phosphorylated form of YAP to that for total YAP in such blots was also calculated and expressed relative to the corresponding value for crypts of control mice (right panel). (D) Cytoplasmic (Cyto) and nuclear (Nuc) fractions prepared from ileal crypts of 8-week-old control or Csk CKO mice were subjected to immunoblot analysis with antibodies to YAP, to lamin A/C (nuclear marker), and to β-tubulin (cytoplasmic marker). (E) Quantitative RT-PCR analysis of *Areg* mRNA in crypts from the small intestine of 8-week-old control or Csk CKO mice. The amount of *Areg* mRNA was normalized by that of GAPDH mRNA and then expressed relative to the normalized value for control mice. (F) Intestinal organoids derived from the jejunum of 8-week-old control or Csk CKO mice were cultured for 2 days, lysed, and subjected to immunoblot analysis with antibodies to YAP and to β-tubulin as for panel A. (G) Intestinal organoids cultured for 2 days as for panel F were subjected to immunostaining with antibodies to YAP (red) as well as to staining with DAPI (blue). Boxed regions in the left images are shown at higher magnification in the right images. Scale bars, 100 μm (left images) and 20 μm (right images). Arrows indicate strong nucleus staining for YAP. (H) Intestinal organoids cultured for 4 days in the absence (−) or presence (+) of NSC23766 (NSC) (100 μM) were lysed and subjected to immunoblot analysis as for panel F. Quantitative data (A, C, E, F, and H) are means ± SEM from at least three independent experiments. *, $P < 0.05$; **, $P < 0.01$ (Student's *t* test).

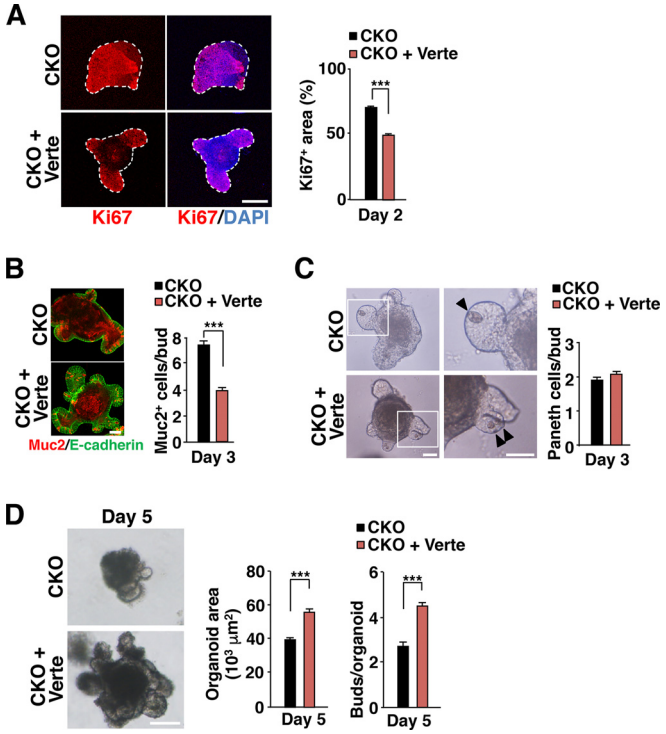

FIG 8 Effects of the YAP inhibitor verteporfin on the phenotypes of Csk-deficient intestinal organoids. (A) Intestinal organoids from the jejunum of 8-week-old Csk CKO mice were cultured in the absence or presence of verteporfin (Verte) (1 μM) for 2 days and then subjected to immunostaining with antibodies to Ki67 (red) and to staining of nuclei with DAPI (blue) (left panel). Dashed lines indicate the boundary of intestinal organoids. Scale bar, 100 μm. The Ki67-positive area was also determined as a percentage of the total organoid area in such images (right panel). (B) Intestinal organoids cultured as for panel A for 3 days were subjected to immunostaining with antibodies to mucin 2 (red) and to E-cadherin (green) (left panel). Scale bar, 50 μm. The number of mucin 2-positive cells per bud was also determined in such images (right panel). (C) Intestinal organoids cultured as for panel A were examined by light microscopy at 3 days after plating (left panel). Boxed regions in the left images are shown at higher magnification in the right images. Arrowheads indicate granule-containing Paneth cells. Scale bars, 50 μm. The number of granule-containing Paneth cells per bud was also determined in such images (right panel). (D) Intestinal organoids cultured as for panel A were examined by light microscopy at 5 days after plating (left panel). Scale bar, 100 μm. The organoid area (middle panel) and the number of buds per organoid (right panel) were also determined in such images. Quantitative data are means ± SEM for a total of 75 organoids (A and D [middle panel]), 45 buds (B), 60 buds (C), or 60 organoids (D [right panel]) per group in three separate experiments. ***, $P < 0.001$ (Student's *t* test).

of SFKs, as well as tyrosine-phosphorylated proteins overall, were localized specifically along the apical surface of IECs (including TA cells and ISCs) in crypts of Csk CKO mice. SFKs are thought to be localized predominantly at lipid rafts (29, 44), and we found that the ganglioside GM1, a marker for lipid rafts (29, 30), was also enriched and localized along the apical surface of crypt IECs. Lipid rafts may therefore recruit SFKs to the apical surface of crypt IECs.

Our results suggest that activated SFKs in crypts of Csk CKO mice promote the activation of FAK by mediating its phosphorylation at Tyr^{576} and Tyr^{577}. Activated FAK in turn forms a complex with c-Src and thereby promotes the tyrosine phosphorylation of other signaling molecules such as p130Cas, which results in activation of Rac (32). Indeed, the activity of Rac was markedly increased in crypts isolated from Csk CKO mice. Furthermore, treatment with a Rac inhibitor suppressed the increased proliferative activity and rescued the imbalance in secretory cell populations (the reduction in Paneth cell number and increase in goblet cell number) apparent in Csk-deficient intestinal organoids. Rac thus likely functions downstream of FAK in the SFK-driven proliferation and differentiation of IECs in intestinal crypts.

YAP is thought to promote cell proliferation and differentiation by regulating the expression of its target genes in various cell types, including IECs (37, 38). Indeed, YAP was previously shown to be predominantly expressed in crypts of the small intestine (45). We found that the amount of YAP was markedly increased in both cytoplasmic and nuclear fractions of crypts isolated from the ileum of Csk CKO mice as well as in cultured organoids from these animals. Consistent with these findings, expression of the YAP target gene *Areg* was significantly increased in crypts of Csk CKO mice. In addition, treatment with a YAP inhibitor attenuated the increased proliferative activity as well as the increase in the number of goblet cells characteristic of Csk-deficient intestinal organoids, implicating YAP in the SFK-induced proliferation of crypt cells and differentiation of goblet cells. The level of YAP phosphorylation at Ser^{381} was markedly reduced in crypts of Csk CKO mice, suggesting that the increase in the amount of YAP protein in IECs of the mutant animals may be attributable to a reduced rate of YAP degradation. The upregulation of YAP protein abundance in Csk-deficient organoids was significantly attenuated by treatment with the Rac inhibitor NSC23766, suggesting that hyperactivation of Rac contributes to this effect. Our results thus suggest that SFKs promote the proliferation of crypt IECs by activating Rac, which in turn upregulates the abundance of YAP. The Rho family GTPases Rac and Rho are thought to contribute to YAP activation by oncogenic mutants of GNAQ in a manner dependent on actin polymerization (46). Phosphorylation of YAP at Tyr^{357} by c-Src increases the stability of the protein, and this action of c-Src has been implicated in the promotion of IEC proliferation (47). Such tyrosine phosphorylation by c-Src of YAP was demonstrated to occur under mucosal injury of the intestine (47). In contrast, we failed to detect the phosphorylation of YAP at Tyr^{357} in crypts isolated from the small intestine of either control or Csk CKO mice under the steady-state condition (see Fig. S8B in the supplemental material).

We also detected cross talk between SFK-mediated signaling and both the Wnt–β-catenin and Notch signaling pathways in IECs. We thus found that the expression of Wnt target genes (*Lgr5*, *Ascl2*, and *Axin2*) was downregulated in crypts of Csk CKO mice. The Wnt–β-catenin signaling pathway is essential for generation and maintenance of ISCs as well as of Paneth cells (1, 2). Consistent with the observed downregulation of Wnt target gene expression, the numbers of ISCs and Paneth cells were reduced in intestinal crypts as well as in intestinal organoids of Csk CKO mice. These results suggest that SFKs negatively regulate Wnt–β-catenin signaling. Given that YAP is thought to inhibit the Wnt–β-catenin signaling pathway (48–50), SFKs likely target this pathway through upregulation of YAP activity in crypt IECs. We also found that IEC-specific ablation of Csk increased the number of goblet cells in the ileum as well as in intestinal organoids and that expression of the Notch target genes *Olfm4* and *Hes1* (9, 51) was downregulated in crypts of Csk CKO mice (Fig. 2E; and see Fig. S4B in the supplemental material). Treatment with inhibitors of Rac or YAP prevented the increase in the number of goblet cells in

Csk-deficient intestinal organoids. Given that the Notch signaling pathway regulates the absorptive versus secretory fate decision in the intestinal epithelium (1, 2, 10), these results thus suggest that SFKs inhibit Notch signaling through activation of Rac or YAP and thereby promote the conversion of TA cells into goblet cells in the intestine. Rac1 and Rac2 contribute to the inhibition of Notch signaling in T lymphocytes during early thymic development (52), suggesting that SFKs might also suppress the Notch pathway through activation of Rac in crypt IECs.

In summary, our results implicate SFKs in the regulation of IEC proliferation and differentiation under the steady-state condition, with both Rac and YAP likely contributing to such regulation downstream of SFKs. Further studies are warranted to clarify the mechanisms by which SFKs regulate Rac and YAP and by which they engage in cross talk with the Wnt–β-catenin and Notch signaling pathways.

ACKNOWLEDGMENTS

We thank M. Okada (Osaka University) for the *Csk*$^{fl/fl}$ mice and helpful discussion, T. Sato (Keio University) for technical advice, and C. J. Kuo (Stanford University) for providing HEK293T cells expressing R-spondin1–Fc.

We declare that we have no conflict of interest.

FUNDING INFORMATION

This work, including the efforts of Takashi Matozaki, was funded by Japan Society for the Promotion of Science (JSPS) (26291022). This work, including the efforts of Takashi Matozaki, was funded by Japan Society for the Promotion of Science (JSPS) (26670142). This work, including the efforts of Yoji Murata, was funded by Japan Society for the Promotion of Science (JSPS) (25460366). This work, including the efforts of Yoji Murata, was funded by Japan Society for the Promotion of Science (JSPS) (16K08624). This work, including the efforts of Takenori Kotani, was funded by Japan Society for the Promotion of Science (JSPS) (25114709).

REFERENCES

1. **Barker N.** 2014. Adult intestinal stem cells: critical drivers of epithelial homeostasis and regeneration. Nat Rev Mol Cell Biol **15:**19–33. http://dx.doi.org/10.1038/nrm3721.
2. **Clevers H.** 2013. The intestinal crypt, a prototype stem cell compartment. Cell **154:**274–284. http://dx.doi.org/10.1016/j.cell.2013.07.004.
3. **Günther C, Martini E, Wittkopf N, Amann K, Weigmann B, Neumann H, Waldner MJ, Hedrick SM, Tenzer S, Neurath MF, Becker C.** 2011. Caspase-8 regulates TNF-α-induced epithelial necroptosis and terminal ileitis. Nature **477:**335–339. http://dx.doi.org/10.1038/nature10400.
4. **Welz PS, Wullaert A, Vlantis K, Kondylis V, Fernández-Majada V, Ermolaeva M, Kirsch P, Sterner-Kock A, van Loo G, Pasparakis M.** 2011. FADD prevents RIP3-mediated epithelial cell necrosis and chronic intestinal inflammation. Nature **477:**330–334. http://dx.doi.org/10.1038/nature10273.
5. **Solanas G, Batlle E.** 2011. Control of cell adhesion and compartmentalization in the intestinal epithelium. Exp Cell Res **317:**2695–2701. http://dx.doi.org/10.1016/j.yexcr.2011.07.019.
6. **Meineke FA, Potten CS, Loeffler M.** 2001. Cell migration and organization in the intestinal crypt using a lattice-free model. Cell Prolif **34:**253–266. http://dx.doi.org/10.1046/j.0960-7722.2001.00216.x.
7. **Sato T, van Es JH, Snippert HJ, Stange DE, Vries RG, van den Born M, Barker N, Shroyer NF, van de Wetering M, Clevers H.** 2011. Paneth cells constitute the niche for Lgr5 stem cells in intestinal crypts. Nature **469:**415–418. http://dx.doi.org/10.1038/nature09637.
8. **Gregorieff A, Clevers H.** 2005. Wnt signaling in the intestinal epithelium: from endoderm to cancer. Genes Dev **19:**877–890. http://dx.doi.org/10.1101/gad.1295405.
9. **VanDussen KL, Carulli AJ, Keeley TM, Patel SR, Puthoff BJ, Magness ST, Tran IT, Maillard I, Siebel C, Kolterud Å Grosse AS, Gumucio DL, Ernst SA, Tsai YH, Dempsey PJ, Samuelson LC.** 2012. Notch signaling modulates proliferation and differentiation of intestinal crypt base columnar stem cells. Development **139:**488–497. http://dx.doi.org/10.1242/dev.070763.
10. **Sancho R, Cremona CA, Behrens A.** 2015. Stem cell and progenitor fate in the mammalian intestine: Notch and lateral inhibition in homeostasis and disease. EMBO Rep **16:**571–581. http://dx.doi.org/10.15252/embr.201540188.
11. **Sato T, Vries RG, Snippert HJ, van de Wetering M, Barker N, Stange DE, van Es JH, Abo A, Kujala P, Peters PJ, Clevers H.** 2009. Single Lgr5 stem cells build crypt-villus structures in vitro without a mesenchymal niche. Nature **459:**262–265. http://dx.doi.org/10.1038/nature07935.
12. **Yamashita H, Kotani T, Park JH, Murata Y, Okazawa H, Ohnishi H, Ku Y, Matozaki T.** 2014. Role of the protein tyrosine phosphatase Shp2 in homeostasis of the intestinal epithelium. PLoS One **9:**e92904. http://dx.doi.org/10.1371/journal.pone.0092904.
13. **Heuberger J, Kosel F, Qi J, Grossmann KS, Rajewsky K, Birchmeier W.** 2014. Shp2/MAPK signaling controls goblet/Paneth cell fate decisions in the intestine. Proc Natl Acad Sci U S A **111:**3472–3477. http://dx.doi.org/10.1073/pnas.1309342111.
14. **Holmberg J, Genander M, Halford MM, Anneren C, Sondell M, Chumley MJ, Silvany RE, Henkemeyer M, Frisen J.** 2006. EphB receptors coordinate migration and proliferation in the intestinal stem cell niche. Cell **125:**1151–1163. http://dx.doi.org/10.1016/j.cell.2006.04.030.
15. **Okada M.** 2012. Regulation of the SRC family kinases by Csk. Int J Biol Sci **8:**1385–1397. http://dx.doi.org/10.7150/ijbs.5141.
16. **Cordero JB, Ridgway RA, Valeri N, Nixon C, Frame MC, Muller WJ, Vidal M, Sansom OJ.** 2014. c-Src drives intestinal regeneration and transformation. EMBO J **33:**1474–1491. http://dx.doi.org/10.1002/embj.201387454.
17. **Nada S, Okada M, MacAuley A, Cooper JA, Nakagawa H.** 1991. Cloning of a complementary DNA for a protein-tyrosine kinase that specifically phosphorylates a negative regulatory site of p60c-src. Nature **351:**69–72. http://dx.doi.org/10.1038/351069a0.
18. **Nada S, Yagi T, Takeda H, Tokunaga T, Nakagawa H, Ikawa Y, Okada M, Aizawa S.** 1993. Constitutive activation of Src family kinases in mouse embryos that lack Csk. Cell **73:**1125–1135. http://dx.doi.org/10.1016/0092-8674(93)90642-4.
19. **Schmedt C, Saijo K, Niidome T, Kuhn R, Aizawa S, Tarakhovsky A.** 1998. Csk controls antigen receptor-mediated development and selection of T-lineage cells. Nature **394:**901–904. http://dx.doi.org/10.1038/29802.
20. **Yagi R, Waguri S, Sumikawa Y, Nada S, Oneyama C, Itami S, Schmedt C, Uchiyama Y, Okada M.** 2007. C-terminal Src kinase controls development and maintenance of mouse squamous epithelia. EMBO J **26:**1234–1244. http://dx.doi.org/10.1038/sj.emboj.7601595.
21. **Murata Y, Kotani T, Supriatna Y, Kitamura Y, Imada S, Kawahara K, Nishio M, Daniwijaya EW, Sadakata H, Kusakari S, Mori M, Kanazawa Y, Saito Y, Okawa K, Takeda-Morishita M, Okazawa H, Ohnishi H, Azuma T, Suzuki A, Matozaki T.** 2015. Protein tyrosine phosphatase SAP-1 protects against colitis through regulation of CEACAM20 in the intestinal epithelium. Proc Natl Acad Sci U S A **112:**E4264–E4271. http://dx.doi.org/10.1073/pnas.1510167112.
22. **Murata Y, Mori M, Kotani T, Supriatna Y, Okazawa H, Kusakari S, Saito Y, Ohnishi H, Matozaki T.** 2010. Tyrosine phosphorylation of R3 subtype receptor-type protein tyrosine phosphatases and their complex formations with Grb2 or Fyn. Genes Cells **15:**513–524. http://dx.doi.org/10.1111/j.1365-2443.2010.01398.x.
23. **Mori M, Murata Y, Kotani T, Kusakari S, Ohnishi H, Saito Y, Okazawa H, Ishizuka T, Mori M, Matozaki T.** 2010. Promotion of cell spreading and migration by vascular endothelial-protein tyrosine phosphatase (VE-PTP) in cooperation with integrins. J Cell Physiol **224:**195–204. http://dx.doi.org/10.1002/jcp.22122.
24. **Madison BB, Dunbar L, Qiao XT, Braunstein K, Braunstein E, Gumucio DL.** 2002. *cis* elements of the villin gene control expression in restricted domains of the vertical (crypt) and horizontal (duodenum, cecum) axes of the intestine. J Biol Chem **277:**33275–33283. http://dx.doi.org/10.1074/jbc.M204935200.
25. **Holt PR, Moss SF, Kapetanakis AM, Petrotos A, Wang S.** 1997. Is Ki-67 a better proliferative marker in the colon than proliferating cell nuclear antigen? Cancer Epidemiol Biomarkers Prev **6:**131–135.
26. **van der Flier LG, van Gijn ME, Hatzis P, Kujala P, Haegebarth A, Stange DE, Begthel H, van den Born M, Guryev V, Oving I, van Es JH, Barker N, Peters PJ, van de Wetering M, Clevers H.** 2009. Transcription

factor achaete scute-like 2 controls intestinal stem cell fate. Cell **136:**903–912. http://dx.doi.org/10.1016/j.cell.2009.01.031.

27. **Batlle E, Henderson JT, Beghtel H, van den Born MM, Sancho E, Huls G, Meeldijk J, Robertson J, van de Wetering M, Pawson T, Clevers H.** 2002. β-Catenin and TCF mediate cell positioning in the intestinal epithelium by controlling the expression of EphB/ephrinB. Cell **111:**251–263. http://dx.doi.org/10.1016/S0092-8674(02)01015-2.
28. **Hanke JH, Gardner JP, Dow RL, Changelian PS, Brissette WH, Weringer EJ, Pollok BA, Connelly PA.** 1996. Discovery of a novel, potent, and Src family-selective tyrosine kinase inhibitor. Study of Lck- and FynT-dependent T cell activation. J Biol Chem **271:**695–701.
29. **Galbiati F, Razani B, Lisanti MP.** 2001. Emerging themes in lipid rafts and caveolae. Cell **106:**403–411. http://dx.doi.org/10.1016/S0092-8674(01)00472-X.
30. **Kenworthy AK, Petranova N, Edidin M.** 2000. High-resolution FRET microscopy of cholera toxin B-subunit and GPI-anchored proteins in cell plasma membranes. Mol Biol Cell **11:**1645–1655. http://dx.doi.org/10.1091/mbc.11.5.1645.
31. **Calalb MB, Polte TR, Hanks SK.** 1995. Tyrosine phosphorylation of focal adhesion kinase at sites in the catalytic domain regulates kinase activity: a role for Src family kinases. Mol Cell Biol **15:**954–963. http://dx.doi.org/10.1128/MCB.15.2.954.
32. **Huveneers S, Danen EH.** 2009. Adhesion signaling—crosstalk between integrins, Src and Rho. J Cell Sci **122:**1059–1069. http://dx.doi.org/10.1242/jcs.039446.
33. **Choma DP, Milano V, Pumiglia KM, DiPersio CM.** 2007. Integrin α3β1-dependent activation of FAK/Src regulates Rac1-mediated keratinocyte polarization on laminin-5. J Investig Dermatol **127:**31–40. http://dx.doi.org/10.1038/sj.jid.5700505.
34. **Frame MC.** 2002. Src in cancer: deregulation and consequences for cell behaviour. Biochim Biophys Acta **1602:**114–130.
35. **Silva CM.** 2004. Role of STATs as downstream signal transducers in Src family kinase-mediated tumorigenesis. Oncogene **23:**8017–8023. http://dx.doi.org/10.1038/sj.onc.1208159.
36. **Gao Y, Dickerson JB, Guo F, Zheng J, Zheng Y.** 2004. Rational design and characterization of a Rac GTPase-specific small molecule inhibitor. Proc Natl Acad Sci U S A **101:**7618–7623. http://dx.doi.org/10.1073/pnas.0307512101.
37. **Yu FX, Zhao B, Guan KL.** 2015. Hippo pathway in organ size control, tissue homeostasis, and cancer. Cell **163:**811–828. http://dx.doi.org/10.1016/j.cell.2015.10.044.
38. **Imajo M, Ebisuya M, Nishida E.** 2015. Dual role of YAP and TAZ in renewal of the intestinal epithelium. Nat Cell Biol **17:**7–19. http://dx.doi.org/10.1038/ncb3084.
39. **Zhao B, Li L, Tumaneng K, Wang CY, Guan KL.** 2010. A coordinated phosphorylation by Lats and CK1 regulates YAP stability through $SCF^{\beta\text{-}TRCP}$. Genes Dev **24:**72–85. http://dx.doi.org/10.1101/gad.1843810.
40. **Zhao B, Wei X, Li W, Udan RS, Yang Q, Kim J, Xie J, Ikenoue T, Yu J, Li L, Zheng P, Ye K, Chinnaiyan A, Halder G, Lai ZC, Guan KL.** 2007. Inactivation of YAP oncoprotein by the Hippo pathway is involved in cell contact inhibition and tissue growth control. Genes Dev **21:**2747–2761. http://dx.doi.org/10.1101/gad.1602907.
41. **Hansen CG, Moroishi T, Guan KL.** 2015. YAP and TAZ: a nexus for Hippo signaling and beyond. Trends Cell Biol **25:**499–513. http://dx.doi.org/10.1016/j.tcb.2015.05.002.
42. **Zhang J, Ji JY, Yu M, Overholtzer M, Smolen GA, Wang R, Brugge JS, Dyson NJ, Haber DA.** 2009. YAP-dependent induction of amphiregulin identifies a non-cell-autonomous component of the Hippo pathway. Nat Cell Biol **11:**1444–1450. http://dx.doi.org/10.1038/ncb1993.
43. **Liu-Chittenden Y, Huang B, Shim JS, Chen Q, Lee SJ, Anders RA, Liu JO, Pan D.** 2012. Genetic and pharmacological disruption of the TEAD-YAP complex suppresses the oncogenic activity of YAP. Genes Dev **26:**1300–1305. http://dx.doi.org/10.1101/gad.192856.112.
44. **Liang X, Nazarian A, Erdjument-Bromage H, Bornmann W, Tempst P, Resh MD.** 2001. Heterogeneous fatty acylation of Src family kinases with polyunsaturated fatty acids regulates raft localization and signal transduction. J Biol Chem **276:**30987–30994. http://dx.doi.org/10.1074/jbc.M104018200.
45. **Camargo FD, Gokhale S, Johnnidis JB, Fu D, Bell GW, Jaenisch R, Brummelkamp TR.** 2007. YAP1 increases organ size and expands undifferentiated progenitor cells. Curr Biol **17:**2054–2060. http://dx.doi.org/10.1016/j.cub.2007.10.039.
46. **Feng X, Degese MS, Iglesias-Bartolome R, Vaque JP, Molinolo AA, Rodrigues M, Zaidi MR, Ksander BR, Merlino G, Sodhi A, Chen Q, Gutkind JS.** 2014. Hippo-independent activation of YAP by the *GNAQ* uveal melanoma oncogene through a trio-regulated rho GTPase signaling circuitry. Cancer Cell **25:**831–845. http://dx.doi.org/10.1016/j.ccr.2014.04.016.
47. **Taniguchi K, Wu LW, Grivennikov SI, de Jong PR, Lian I, Yu FX, Wang K, Ho SB, Boland BS, Chang JT, Sandborn WJ, Hardiman G, Raz E, Maehara Y, Yoshimura A, Zucman-Rossi J, Guan KL, Karin M.** 2015. A gp130-Src-YAP module links inflammation to epithelial regeneration. Nature **519:**57–62. http://dx.doi.org/10.1038/nature14228.
48. **Barry ER, Morikawa T, Butler BL, Shrestha K, de la Rosa R, Yan KS, Fuchs CS, Magness ST, Smits R, Ogino S, Kuo CJ, Camargo FD.** 2013. Restriction of intestinal stem cell expansion and the regenerative response by YAP. Nature **493:**106–110. http://dx.doi.org/10.1038/nature11693.
49. **Imajo M, Miyatake K, Iimura A, Miyamoto A, Nishida E.** 2012. A molecular mechanism that links Hippo signalling to the inhibition of Wnt/β-catenin signalling. EMBO J **31:**1109–1122. http://dx.doi.org/10.1038/emboj.2011.487.
50. **Gregorieff A, Liu Y, Inanlou MR, Khomchuk Y, Wrana JL.** 2015. Yap-dependent reprogramming of $Lgr5^{+}$ stem cells drives intestinal regeneration and cancer. Nature **526:**715–718. http://dx.doi.org/10.1038/nature15382.
51. **Jarriault S, Brou C, Logeat F, Schroeter EH, Kopan R, Israel A.** 1995. Signalling downstream of activated mammalian Notch. Nature **377:**355–358. http://dx.doi.org/10.1038/377355a0.
52. **Dumont C, Corsoni-Tadrzak A, Ruf S, de Boer J, Williams A, Turner M, Kioussis D, Tybulewicz VL.** 2009. Rac GTPases play critical roles in early T-cell development. Blood **113:**3990–3998. http://dx.doi.org/10.1182/blood-2008-09-181180.